1

Active Wave Experiments in Space Plasmas: The Z Mode

R.F. Benson[1], P.A. Webb[1], J.L. Green[1], D.L. Carpenter[2], V.S. Sonwalkar[3], H.G. James[4], and B.W. Reinisch[5]

[1] NASA/Goddard Space Flight Center, Greenbelt, MD USA
Robert.F.Benson@nasa.gov
[2] Stanford University, California USA
[3] University of Alaska Fairbanks, Alaska USA
[4] Communications Research Centre, Toronto, Canada
[5] University of Massachusetts Lowell, Massachusetts USA

Abstract. The term Z mode is space physics notation for the low-frequency branch of the extraordinary (X) mode. It is an internal, or trapped, mode of the plasma confined in frequency between the cutoff frequency f_z and the upper-hybrid frequency f_{uh} which is related to the electron plasma frequency f_{pe} and the electron cyclotron frequency f_{ce} by the expression $f_{uh}^2 = f_{pe}^2 + f_{ce}^2$; f_z is a function of f_{pe} and f_{ce}. These characteristic frequencies are directly related to the electron number density N_e and the magnetic field strength $|\mathbf{B}|$, i.e., $f_{pe}(\mathrm{kHz})^2 \approx 80.6 N_e(\mathrm{cm}^{-3})$ and $f_{ce}(\mathrm{kHz})^2 \approx 0.028|\mathbf{B}|(\mathrm{nT})$. The Z mode is further classified as slow or fast depending on whether the phase velocity is lower or higher than the speed of light in vacuum. The Z mode provides a link between the short wavelength λ (large wave number $k = 2\pi/\lambda$) electrostatic (es) domain and the long λ (small k) electromagnetic (em) domain. An understanding of the generation, propagation and reception of Z-mode waves in space plasma leads to fundamental information on wave/particle interactions, N_e, and field-aligned N_e irregularities (FAI) in both active and passive wave experiments. Here we review Z-mode observations and their interpretations from both radio sounders on rockets and satellites and from plasma-wave receivers on satellites. The emphasis will be on the scattering and ducting of sounder-generated Z-mode waves by FAI and on the passive reception of Z-mode waves generated by natural processes such as Cherenkov and cyclotron emission. The diagnostic applications of the observations to understanding ionospheric and magnetospheric plasma processes and structures benefit from the complementary nature of passive and active plasma-wave experiments.

Key words: Auroral kilometric radiation, Z-mode, free space radiation, wave transformation, radiation escape, cavity modes, active experiments

R.F. Benson et al.: *Active Wave Experiments in Space Plasmas: The Z Mode*, Lect. Notes Phys. **687**, 3–35 (2006)
www.springerlink.com

1.1 Introduction

According to cold plasma theory, at high frequencies there are two characteristic electromagnetic (em) waves, or modes, that can propagate in a magnetoplasma. They are often referred to as the free-space ordinary (O) and extraordinary (X) modes because waves propagating in these modes can smoothly connect to free space. The X mode has two branches. In addition to the free-space mode, it has a mode called the slow branch. This name is used because it is restricted to propagation velocities less than the vacuum speed of light c. Since this mode only exists within a plasma, there was considerable interest in explaining observations indicating that it was responsible for a unique signature on early ground-based radars designed to probe the ionosphere. In their most common application these radars, called ionosondes, operate by transmitting a radio pulse of short time duration at a particular frequency and receiving, at the same frequency, for a time interval sufficient to receive an echo from the ionosphere overhead. This process is repeated over a range of frequencies likely to produce reflections. The resulting record is called an ionogram.

Normally, there are two ionospheric reflections, one due to the O mode and one due to the X mode. "On rare occasions", as first reported by Eckersley [23], there is a third reflection with the same polarization as the O mode. This third reflection trace, corresponding to the slow X-mode branch, was dubbed the Z mode in ionospheric research; a designation commonly used in space physics. In order to explain the presence of the Z mode at ground level, i.e., far below the ionospheric plasma, and the polarization (same as the O mode), a Z-O mode coupling process involving obliquely-propagating O-mode waves was introduced by Ellis [24] as discussed in Sect. 13.5 of Ratcliffe [57]. An ionogram showing this triple splitting of the ionospheric reflection is schematically illustrated in Fig. 1.1. Here the apparent height h' (or apparent, or virtual, range) corresponds to $ct/2$, where t is the round trip echo delay time, and the frequency f is the sounding frequency. For a description of the sounding technique, and the inversion from $h'(f)$ to $N_e(h)$, where N_e is the electron number density and h is the true altitude, see Thomas [64] and Reinisch [58] and references therein.

In order to understand how the Z mode is related to the free-space O and X modes it is necessary to discuss plasma-wave dispersion. This topic will be addressed in Sect. 1.2. Since the Z mode is an internal (or trapped) mode of the plasma, the emphasis in this paper will be on the reception of the Z mode by space-borne receivers during active and passive experiments. Sections 1.3 and 1.4 will deal with sounder-stimulated Z-mode waves in the ionosphere and the magnetosphere, respectively. Particular attention will be given to the information that the sounder-stimulated Z-mode waves provide concerning magnetic-field aligned N_e irregularities (FAI). FAI are irregularities in N_e transverse to the direction of the background magnetic field $\mathbf{B}$ that are maintained for long distances along $\mathbf{B}$. They efficiently scatter and

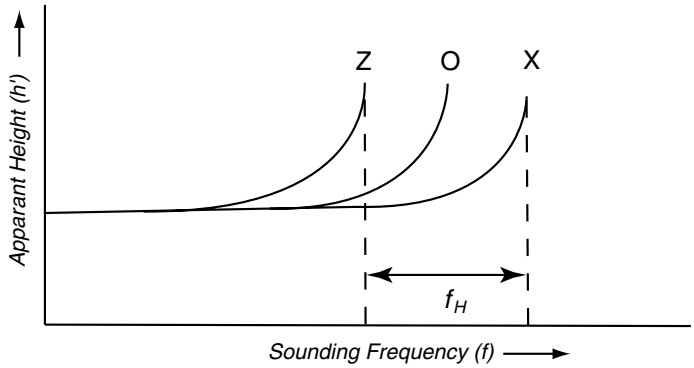

Fig. 1.1. Ground-based ionogram schematic illustrating Z-, O-, and X-mode reflection traces. Here the ionospheric notation for the electron cyclotron frequency, f_H, is used [adapted from 57]

duct sounder-stimulated Z-mode waves. Section 1.5 discusses a combined active/passive investigation of Z-mode waves generated by natural processes. A summary is presented in Sect. 1.6.

There have been many spacecraft that have generated Z-mode waves in the ionosphere and magnetosphere using radio sounders. Similarly, there have been many satellites that have detected Z-mode waves of magnetospheric origin using plasma wave receivers [LaBelle and Treumann, 43, included a review of auroral Z-mode observations and theory]. Our goal is not to review the Z-mode observations from all of these missions. Rather, it is to select specific examples that illustrate the range of Z-mode phenomena observed in active space wave-injection experiments and to demonstrate their diagnostic capability. In the case of the ionosphere, we will mainly use data from two missions, namely, (1) the ISIS (International Satellites for Ionospheric Studies) satellites [Jackson and Warren, 33] and (2) the OEDIPUS sounding rocket double payloads (Observations by Electric-field Determinations in the Ionospheric Plasma-A Unique Strategy) [see, e.g., 30, 36]. In the case of the magnetosphere, data from the Radio Plasma Imager (RPI) [Reinisch et al., 59] on the IMAGE (Imager for Magnetopause-to-Aurora Global Exploration) satellite [Burch, 15] will be used.

1.2 Plasma Wave Dispersion

Waves in a cold plasma are described by a dispersion relation, i.e., the scalar relation expressing the angular frequency $\omega = 2\pi f$ in terms of the propagation vector $\mathbf{k}$, which is related to the refractive index $\mathbf{n}$ by $\mathbf{n} = \mathbf{k}c/\omega$ where $k = |\mathbf{k}| = (2\pi/\lambda)$ and λ is the wavelength.This description has been given in a number of books and review papers [see, e.g., 1, 19, 27, 39, 57, 63]. Figure 1.2 presents dispersion curves for waves propagating in a homogeneous cold

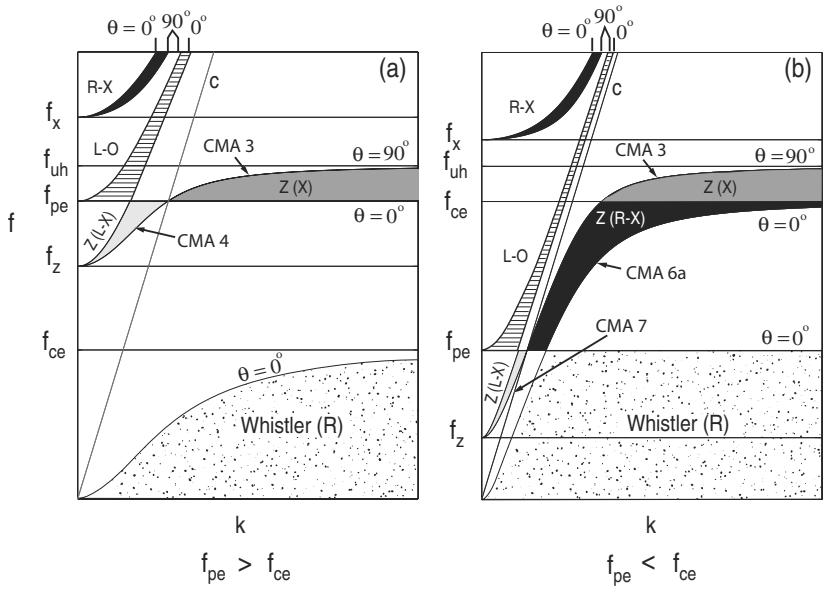

Fig. 1.2. Schematic dispersion diagrams. (**a**) Example when $f_{pe}/f_{ce} > 1$. (**b**) Example when $f_{pe}/f_{ce} < 1$ [adapted from 27, 62] (Reprinted with permission of the American Geophysical Union)

plasma, where ion motions are neglected, with **k** making an angle θ relative to **B**. The figure shows the dispersion curves for $\theta = 0$ and $\theta = \pi/2$ cases for a range of frequency and wave number. The region between these two limiting cases is shown by various shades of gray – indicating various modes – where the propagation at oblique wave normal angles is permitted. The waves are labelled based on their polarization for parallel or perpendicular propagation, i.e., R or L for right- or left-hand polarization (with respect to the direction of **B**) when $\theta = 0$, and X or O for extraordinary and ordinary mode polarization when $\theta = \pi/2$. In some regions, only one letter is used indicating that propagation is not possible for both $\theta = 0$ and $\theta = \pi/2$. Thus Z(X) indicates that the Z mode does not include the condition $\theta = 0$ in the region indicated based on the cold-plasma approximation. The Z-mode regions in Fig. 1.2 are also labelled with the CMA designation using the notation of Stix [63]. Thus Z(X) occurs in CMA region 3 where k, and thus $n = |\mathbf{n}|$, can become large leading to a condition ($n = \infty$) known as *resonance*; the condition $k = 0$ (or $n = 0$) is known as a *cutoff*.

The plasma resonances and cutoffs in Fig. 1.2 are given by the following expressions:

$$f_{ce}(\mathrm{kHz}) = \frac{|e|}{2\pi m_e)}|\mathrm{B}| \approx 0.028\,|\mathbf{B}(\mathrm{nT})| \tag{1.1}$$

$$f_{pe}(\text{kHz}) = \frac{e^2}{(4\pi^2\epsilon_0 m_e)}^{\frac{1}{2}} N_e^{\frac{1}{2}} \approx 80.6\ N_e(\text{cm}^{-3})^{\frac{1}{2}} \tag{1.2}$$

$$f_{uh} = (f_{pe}^2 + f_{ce}^2)^{\frac{1}{2}} \tag{1.3}$$

$$f_x = \frac{f_{ce}}{2}\left[1 + \left(1 + 4\frac{f_{pe}^2}{f_{ce}^2}\right)^{\frac{1}{2}}\right] \tag{1.4}$$

$$f_z = \frac{f_{ce}}{2}\left[-1 + \left(1 + 4\frac{f_{pe}^2}{f_{ce}^2}\right)^{\frac{1}{2}}\right] \equiv f_x - f_{ce} \tag{1.5}$$

where e is the electron charge, m_e is the electron mass and ϵ_0 is the permittivity of free space. For $\theta < \pi/2$, the resonance condition that replaces (3) above, in CMA 3 of Fig. 1.2, is known as the Z-infinity and is given by

$$f_{ZI} = \frac{1}{\sqrt{2}}\left[\left(f_{uh}^2 + (f_{uh}^4 - 4f_{ce}^2 f_{pe}^2 \cos^2\theta)^{\frac{1}{2}}\right)\right]^{\frac{1}{2}} \tag{1.6}$$

The Z infinity is also referred to as the upper oblique resonance [see, e.g., Beghin et al., 4]. The above cutoffs and resonances are described using different notations in Sects. 6.4 and 6.5 of Ratcliffe [57] and Sects. 1–5 of Stix [63].

Figure 1.2 is often presented in the form of ω vs. k. In this presentation the magnitudes of the phase and group velocities,

$$|\mathbf{v}_p| = \left|\frac{\omega}{\mathbf{k}}\right| \tag{1.7}$$

and

$$|\mathbf{v}_g| = \left|\frac{\partial\omega}{\partial\mathbf{k}}\right|, \tag{1.8}$$

respectively, correspond to the slope of the line from the origin to a particular point on a dispersion curve, and to the slope of a line tangent to the dispersion curve at that point, respectively. In Fig. 1.2 there is a slanting line labelled c to indicate that it corresponds to free-space propagation. The curves to the left of this line (labelled R-X, L-O and L-X) have $v_p \geq c$ and those to the right have $v_p < c$. Accordingly, the Z-mode waves labelled L-X are called fast Z (CMA 4 in Fig. 1.2a and CMA 7 in Fig. 1.2b) and those labelled Z(X) are called slow Z (CMA 3 in Figs. 1.2a and 2b). Both fast and slow Z-mode waves can be found in the region labelled R-X (CMA 6a in Fig. 1.2b).

The ionosphere and magnetosphere, contrary to the conditions appropriate to Fig. 1.2, are neither homogeneous nor cold and the ions are not motionless. Yet the dispersion properties derived by using these assumptions, and illustrated by Fig. 1.2, have proved very successful in describing many phenomena. The standard approach is to consider the ionosphere as a horizontally-stratified medium with N_e varying only in the vertical direction. Then the wave is considered to behave as if it were in a homogeneous medium at each

ionospheric level. Both diagrams in Fig. 1.2 correspond to a specific value of f_{pe}/f_{ce}. The curves change shape as f_{pe}/f_{ce} changes. For example, in Fig. 1.2a, the band of no propagation between f_{ce} and f_Z only appears when $f_{pe}/f_{ce} > \sqrt{2}$. Also, the Z(X) region, i.e., CMA-region 3 in Figs. 1.2a and 1.2b, is maximum for the condition $f_{pe} = f_{ce}$.

The progress of a radio wave through the non-homogeneous ionosphere can be modelled by considering the change in the shape of the refractive-index surface as f_{pe}/f_{ce} changes. This process is illustrated in Fig. 1.3 to illustrate how Z-mode signals at a frequency f from a high-latitude source of natural origin could propagate over great distances in the horizontal direction. The conditions correspond to a source location where $f \approx f_{pe} < f_{ce}$. The left side of the diagram shows the evolution of the refractive-index surfaces from low to high altitudes corresponding to plasma conditions changing from CMA regions 7 to 6a to 3 in Fig. 1.2b. Gurnett et al. [28] used a construction technique introduced by Poeverlein [54], based on Snell's law, to argue that a wave at frequency f originating in the region where $f < f_{ce}$ will be refracted at the $f = f_{ce}$ level and will be able to propagate long distances in the horizontal direction. In Fig. 1.3, the arrows originating at the intersections of the vertical dashed line with these refractive index surfaces indicate the direction of $\mathbf{v}_g$ in (benson-eq8). Note the change from a closed refractive index surface to an open surface as CMA region 3 is encountered.

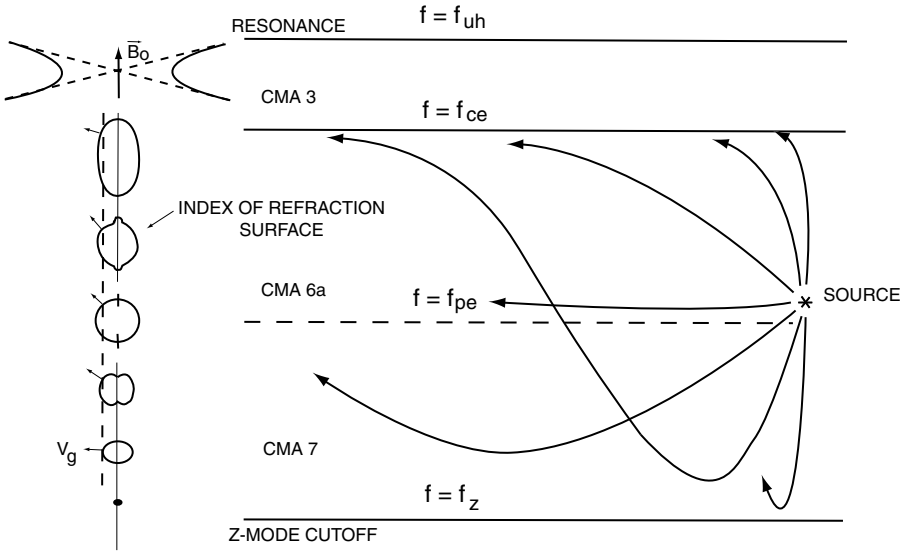

Fig. 1.3. Illustration of the large change in the shape of the refractive-index surface as CMA region 3 is encountered and the ability for long-range horizontal propagation in the Z mode in the polar regions where **B** is nearly vertical [adapted from 28] (Reprinted with permission of the American Geophysical Union)

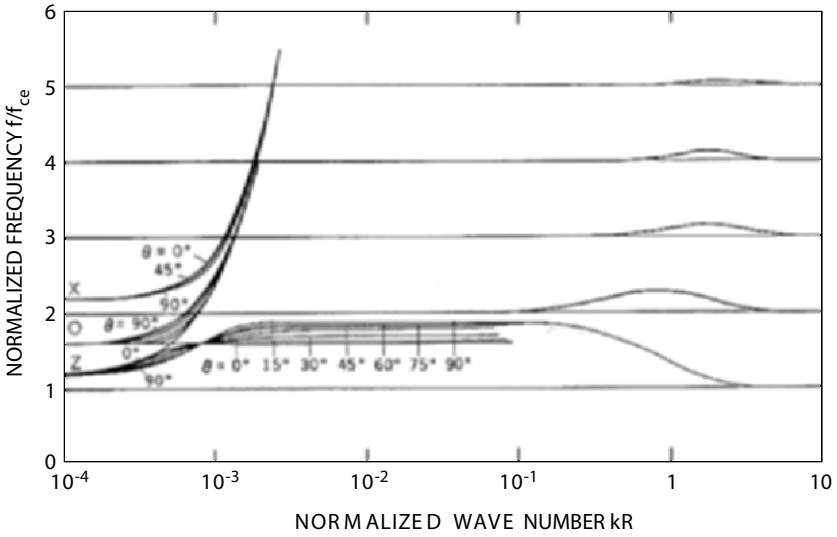

Fig. 1.4. Normalized calculated dispersion diagram for a wide range of wavelengths with electron thermal motions included where f is normalized by f_{ce} and k is normalized by $1/R$ where R is the electron cyclotron radius for the case $f_{pe}/f_{ce} = 1.6$ [adapted from Oya, 53] (Reprinted with permission of the American Geophysical Union)

Figure 1.4 shows the result of numerical solutions of the dispersion relations, for a particular case of $f_{pe}/f_{ce} > 1$, for all θ, and for θ ranging from 0 to $\pi/2$, when hot-plasma effects are included. In these solutions, electron thermal motions are included and a Maxwellian electron velocity distribution function is assumed but collisions are neglected and the ions are still considered to provide an immobile neutralizing background [Oya, 53]. The right portion of the diagram corresponds to the electrostatic (es) domain and the left portion corresponds to the electromagnetic (em) domain. New wave modes, known as the Bernstein modes [Bernstein, 13], now appear between the nf_{ce} harmonics in the *es-domain*. The Bernstein modes correspond to undamped modes with $\theta = \pi/2$. Damping rapidly increases for these modes as θ departs from $\pi/2$. These *es-modes* are coupled to the *em-domain*, with negligible damping, through the Z-mode when $\theta \approx \pi/2$, corresponding to frequencies close to f_{uh}, each, in turn, as f_{uh} increases for increasing f_{pe}/f_{ce} values. Thus the Z-mode near $\theta = \pi/2$, i.e., near f_{uh}, is of prime importance in the coupling of energy resulting from wave/particle interactions in the *es-domain* into the *em-domain* where the information can be transmitted out of the plasma.

1.3 Sounder-Stimulated Z-Mode Waves in the Topside Ionosphere

1.3.1 Single Spacecraft: Vertical and Oblique Propagation

In a space plasma such as the ionosphere the Z mode can be directly detected by ionospheric topside sounders. Figure 1.5a presents an example of a mid-latitude ionogram where ionospheric reflections form a clear Z mode trace in addition to O- and X-mode traces. Also seen in Fig. 1.5a are sounder-stimulated plasma resonances at $f_{ce} = f_H, f_{pe} = f_N, f_{uh} = f_T$ and $2f_{ce} = 2f_H$ and an oblique Z trace labelled Z'. The resonances can be used to accurately determine the ambient $|\mathbf{B}|$ and N_e values from (1.1)–(1.3) as, e.g., given in the reviews of Muldrew [50] and Benson [7].

The presently accepted interpretation for these principal plasma resonances stimulated by ionospheric topside sounders is based on the investigation by Calvert [16] of the Z′ trace. He showed that this trace, which lies between f_{pe} and f_{uh}, is the result of ionospheric reflections of obliquely-propagating Z-mode waves. These oblique reflections result from the shape of the refractive index surfaces, in particular from the change in the shape to form a sphere plus a line parallel to $\mathbf{B}$ when the downward-propagating Z-mode wave encounters the level where $f = f_{pe}$ (see the left side of Fig. 1.3). The Z′ trace is caused by waves reflected at this level. This condition was called a "spitze" by Poeverlein [54] and is discussed in some detail in Budden [14]. The Z′ trace could be explained by using ray tracing with the cold plasma theory.

Calvert [16] did not restrict his calculations to the cold plasma approximation, however, and found ray paths that could return to the spacecraft that included propagation beyond the resonance-cone angle limit of cold plasma theory. These echoes were electrostatic in nature and had echo times much greater than the observed Z′ echoes so the solutions were discarded. McAfee [46], in his investigation of the plasma resonance observed at f_{pe}, found that these hot-plasma solutions had echo delay times comparable to the delays observed on topside ionograms when frequencies very close to f_{pe} were considered. This oblique-echo model was later extended to the plasma resonances observed at f_{uh} [47] and at nf_{ce} [50]. Thus, the investigation of oblique Z-mode propagation by Calvert [16] provided the fundamental first step toward our understanding of sounder-stimulated plasma resonances.

Even though the Z-mode is defined as the slow branch of the X mode, it is important to note that the Z and X modes have comparable group velocities near their respective cutoffs. This behavior is clearly illustrated in Fig. 1.5b. Though Z-mode waves cannot travel as far from the spacecraft as the free-space O- and X-mode waves, they are useful for determining the vertical N_e distribution out to a few hundred km from the spacecraft as seen in Fig. 1.5c. The good agreement between the N_e values obtained in Fig. 1.5c by inverting the Z-, O- and X-mode ionospheric-reflection traces of Fig. 1.5a provides

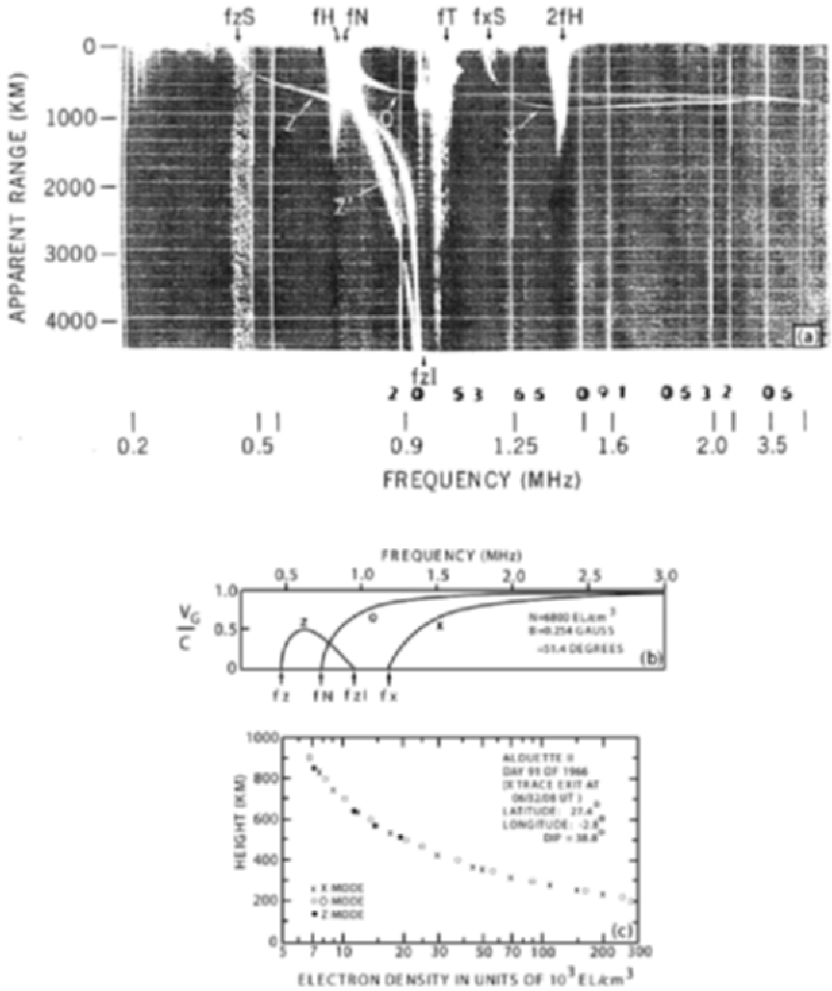

Fig. 1.5. (**a**) Alouette-2 mid-latitude ionogram, in negative format with signal reception in white on a black background, showing Z, O and X traces. Here the ionospheric notation of H, N, and T is used to represent the subscripts ce, pe, and uh, respectively, in the present work. Also, "S" is used to designate the cutoff frequencies at the satellite. The f_{zI} label and arrow below the ionogram, and near the 0.9 MHz frequency marker, identifies the Z infinity condition given by (6). (**b**) Corresponding group velocities ($N_e = 6800\,\mathrm{cm}^{-3}$ corresponds to $f_{pe} = 0.74\,\mathrm{MHz}$ from (2), $B = 0.254 = 0.254 \times 10^{-4}\,\mathrm{T} = 0.254 \times 10^{5}\,\mathrm{nT}$ corresponds to $f_{ce} = 0.7112\,\mathrm{MHz}$ from (1) and $f_{uh} = 1.026\,\mathrm{MHz}$ from (3)). (**c**) Calculated N_e values from each of the traces [adapted from Jackson, 32]

confidence that the two main assumptions used in the inversion process, namely, vertical propagation and a horizontally-stratified ionosphere, were justified since this process is independent for each trace [Jackson, 32].

For vertical propagation the propagation angle relative to **B** is 90°-dip angle, or $\phi = 51.4°$ using Jackson's notation of Fig. 1.5b. Using this ϕ value in (6), with the other values from Fig. 1.5b where $f_{pe}/f_{ce} = 1.04$, yields $f_{ZI} = 0.968$ MHz in agreement with the observed narrow vertical modulated feature observed from zero to approximately 3,000 km apparent range; it is labelled f_{zI} just below the ionogram. This feature can be observed because the wide receiver bandwidth (3 dB bandwidth of 37 kHz) allows long-duration signals returning from the previous pulse (differing by only a few kHz) to be observed at the start of the receiving interval, i.e., it corresponding to a wrap-around of the apparent-range scale for the asymptotic Z-mode echo.

Figure 1.6 shows examples of Z-mode echoes that clearly illustrate the limiting behavior of the Z-mode cold-plasma dispersion curves in Figs. 1.2 and 1.4 for conditions of nearly parallel and nearly perpendicular propagation relative to **B**. In Fig. 1.6a, corresponding to high latitude and thus nearly parallel propagation, the Z- and O-mode traces touch one another near 700 km apparent range and 0.9 MHz suggesting coupling like in the dispersion diagrams in Figs. 1.2 and 1.4 for $\theta = 0$. Also, the Z trace has a large apparent range at this frequency, coinciding with the combined f_{pe} and f_{ce} plasma resonances, as would be expected from (1.6) with $\theta = 0$, i.e., $f_{ZI} = f_{pe} = f_{ce}$. From the observed plasma resonances and wave cutoffs in Fig. 1.6a, and equations (1.3)–(1.5), $f_{pe}/f_{ce} = 0.92/0.935 = 0.98$ for this ionogram. In Fig. 1.6b, corresponding to low latitude and thus perpendicular propagation, the Z-mode trace becomes asymptotic to f_{uh}, again, as expected from (1.6) (now with $\theta = \pi/2$). In this case, $f_{pe}/f_{ce} = 1.89/0.565 = 3.35$. When nearly parallel or nearly perpendicular propagation is involved in the presence of FAI, dramatic ionogram signatures can be produced due to ducting and scattering, respectively, of the sounder-generated Z-mode signals.

1.3.2 Single Spacecraft: Ducted Propagation

When ionospheric topside sounders encounter equatorial plasma bubbles, dramatic floating X-mode echoes are observed that resemble epsilons [Dyson and Benson, 22]. They are called floating because they are not tied to the zero-time baseline at the top of the figure. These traces are the result of sounder-generated signals that echo in both the local and conjugate hemispheres (relative to the location of the satellite) due to ducted propagation in FAI that are maintained from one hemisphere to the other. The bottom portion of Fig. 1.7 illustrates the top segment of such an X-mode epsilon in the frequency range above about 2.9 MHz and at apparent ranges beyond 2200 km. The X-mode echo just above this echo signature, i.e., corresponding to virtual ranges less than 2200 km in the bottom portion of Fig. 1.7, is due to ducted propagation in the local hemisphere. In the top portion of Fig. 1.7 the distances to the

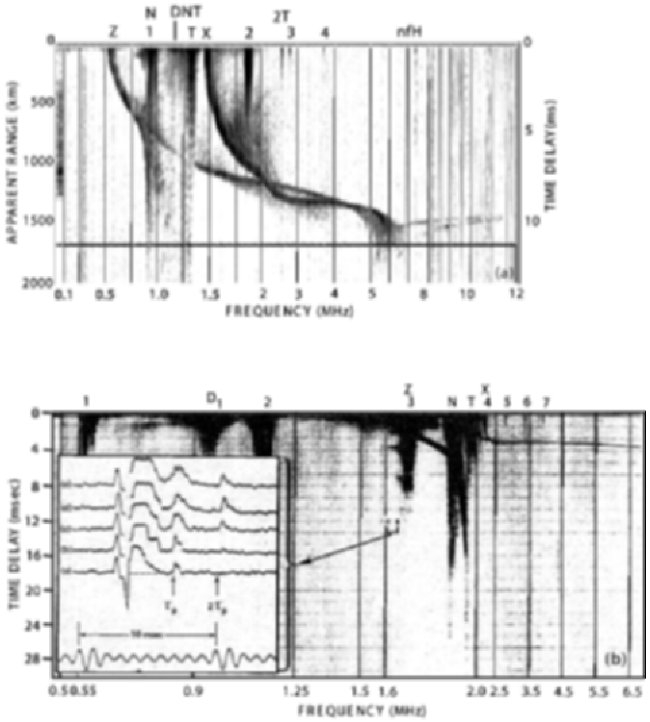

Fig. 1.6. (**a**) ISIS-2 high-latitude ionogram showing Z, O and X traces under conditions of nearly parallel propagation (Resolute Bay digital ionogram obtained from http://nssdc.gsfc.nasa.gov/space/isis/isis-status.html corresponding to 1500:28 UT on day 126 of 1973; 62.8° latitude, −101.8° longitude, 1394 km altitude, 83° dip). (**b**) Low-latitude Alouette-2 ionogram showing Z, O and X traces under conditions of nearly perpendicular propagation [adapted from Benson, 6]. As in Fig. 1.5, the ionospheric notation of N, and T is used to represent the subscripts pe, and uh, respectively, and numerals are used to identify the $nf_H = nf_{ce}$ resonances. The $3f_{ce}$ resonance contains two spurs on the low-frequency side (see Sect. 1.3.6) with delay times near 4 and 7 ms. The insert shows five selected receiver amplitude vs. time traces corresponding to these spur observations. Each trace represents a vertical scan line on the ionogram display, the amplitude modulation on the insert traces corresponding to the intensity modulation on the ionogram scan lines. The initial systematic positive and negative spikes on each of the insert traces are calibration and sync pulses [see Fig. 31 of Franklin and Mclean, 25]; the time-delay zero point was taken as the left side of the dashed line segment on the insert trace labelled (a). The nf_{ce} resonances indicated that $f_{ce} = 0.565$ MHz corresponding to $\tau_p = 3.25$ ms (Reprinted with permission of American Geophysical Union)

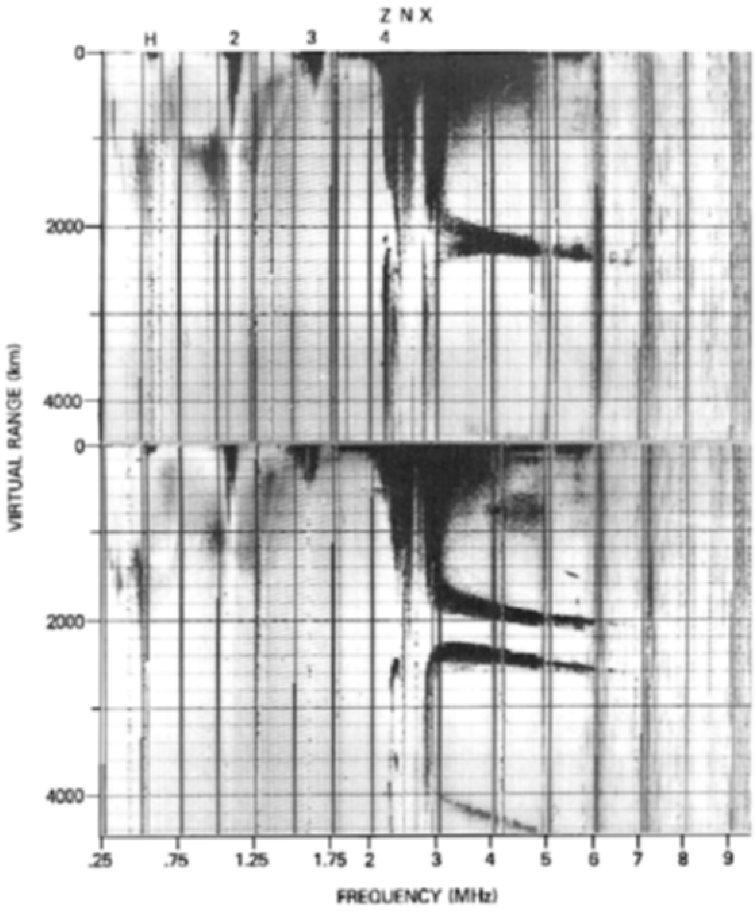

Fig. 1.7. ISIS-1 ionograms recorded 1000 km above the dip equator showing Z- and X-mode echoes from within an equatorial plasma bubble [9]. The ionospheric notation of H, and N is used to represent the subscripts ce and pe, respectively; numerals are used to identify the $nf_H = nf_{ce}$ resonances (Reprinted with permission of American Geophysical Union)

reflection levels in each hemisphere were the same, as the two traces merge and have the same virtual ranges from about 2200 to 2400 km.

Z-mode echoes from waves that are ducted along FAI can form truncated versions of these floating X-mode epsilons. In both portions of Fig. 1.7 the ducted Z-mode waves are confined to a narrow frequency range below the label Z at the top of the figure. As in the case of the ducted X-mode signals, the Z-mode traces tied to the zero virtual-range scale correspond to signals ducted within the local hemisphere and those beyond about 2000 km in virtual range correspond to signals that experience ducted propagation into both

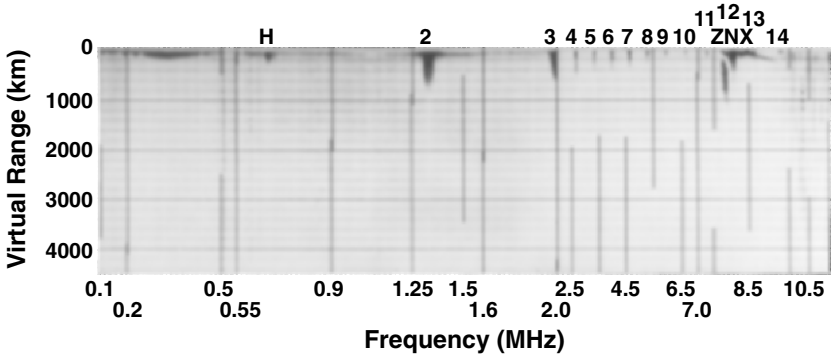

Fig. 1.8. A portion of an Alouette-2 ionogram showing Z-mode floating echoes, attributed to wave ducting in FAI, from f_Z, to a maximum frequency prior to f_{pe} labelled Z and N at the figure, respectively. The label notation is the same as in Fig. 1.7 [adapted from Benson, 9] (Reprinted with permission of the American Geophysical Union)

hemispheres. Note that the ducted Z-mode traces terminate before they reach the local f_{pe}, designated by N at the top of the figure. Similar frequency restrictions of the reception of sounder-stimulated Z-mode waves attributed to wave ducting were commonly observed in an investigation of FAI near 500 km based on Alouette-2 perigee observations [9]; an example is shown in Fig. 1.8.

In a comparison of wave ducting in different wave modes, assuming small propagation angles inside a duct produced by a small increase in refractive index, Calvert [17] showed that under conditions of high N_e, similar to the conditions of Fig. 1.8, Z-mode ducting should be stronger than X- and O-mode ducting. The strongest Z-mode ducting was found to occur in the frequency range from f_Z to midway between f_Z and f_{pe} where a transition from trough ducting to crest ducting occurs due to a curvature reversal in the refractive-index surface. Calvert [17] argues that ducting cannot be maintained across the curvature reversal in agreement with the upper-frequency truncation of the floating Z-mode signals attributed to FAI wave ducting in Fig. 1.7 and Fig. 1.8.

1.3.3 Single Spacecraft: Wave Scattering

Sounder-generated Z-mode waves that are scattered by FAI lead to strong signal returns in the frequency region between the greater of f_{ce} and f_{pe} and less than f_{uh}, i.e., in CMA region 3 in Figs. 1.2 and 1.4. Z-mode ray-tracing calculations indicate that the ray becomes horizontal in the ionosphere as the refractive index tends to infinity [Lockwood, 45] leading to a condition Muldrew [49] termed "wave trapping". The resulting signature is labelled as a noise band in Fig. 1.9. Denisenko et al. [21] used such signatures in the

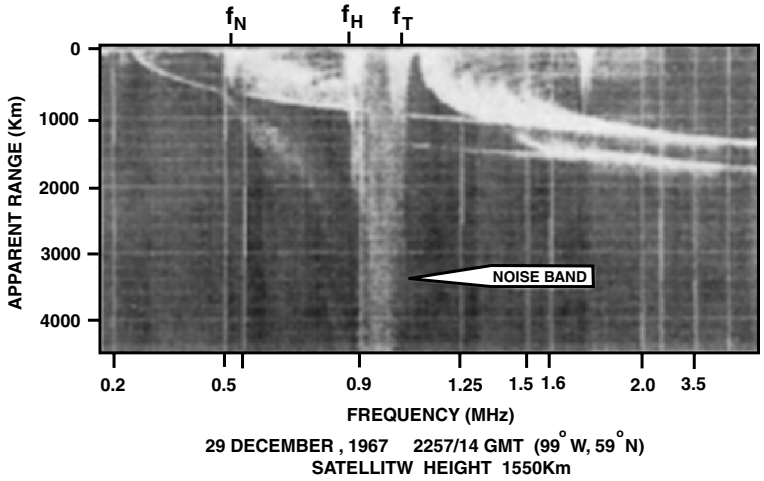

Fig. 1.9. An Alouette-2 ionogram showing sounder-generated Z-mode signal returns attributed to wave scattering in FAI (labelled "noise band") [Muldrew, 49]. The label notation is the same as in Fig. 1.5a (Copyright 1969 by IEEE; reprinted with permission)

COSMOS-1809 topside-sounder data to investigate the global distribution of small-scale (∼10–100 m) FAI in the 940 to 980 km altitude range.

1.3.4 Dual Payloads: Slow Z

The above discussion pertained to observations where the receiver and transmitter were on the same spacecraft and they shared a common antenna. Thus the received Z-mode signals correspond to echo returns either from short distances, due to scattering from FAI in the vicinity of the satellite (Fig. 1.9), or from long distances (∼100's km) due to vertical propagation (Z trace in Fig. 1.5a), oblique propagation (Z′ trace in Fig. 1.5a), or to nearly parallel propagation that is ducted along FAI (Figs. 7 and 8). The Z mode has also been investigated during space experiments involving wave propagation between receivers and transmitters on different payloads.

James [34, 35] performed such experiments during a high-latitude rendezvous between ISIS 1 and ISIS 2. The operating frequency was in the range $f_{pe} < f_{ce} < f < f_{uh}$, i.e., corresponding to "slow Z-mode" propagation in CMA-region 3 of Fig. 1.2b. These waves were observed to propagate over distances of several hundred km. It was found [James, 35] that the observed transmission-reception signal delay times could be explained by ray optics but that the observed distortion of the received pulse relative to the transmitted pulse indicated the importance of signal scattering by FAI.

The OEDIPUS-A dual-payload rocket was launched from the Andøya Rocket range in Norway on January 30, 1989. It was dedicated to such

two-point measurements and provided an additional opportunity to investigate slow Z-mode propagation [James, 36]. In this case, $f_{ce} < f_{pe} < f < f_{uh}$, i.e., corresponding to slow Z-mode propagation in CMA-region 3 of Fig. 1.2a. The transmitting and receiving payloads were separated by nearly 1 km and the separation direction differed from the **B** direction by only a few degrees. The observed delay times for the Z-mode were too large to be explained by free-space propagation and the full *em* solution of the hot plasma dispersion equation, based on the work of Lewis and Keller [44] and Muldrew and Estabrooks [51], was used to investigate the problem. Using this hot-plasma approach, James [36] constructed refractive-index surfaces appropriate to the problem (see Fig. 1.10).

Note how different these hot-plasma Z-mode refractive-index surfaces are from the cold plasma surfaces illustrated on the left side of Fig. 1.3 in the CMA-region 3. James [36] found that direct ray paths connecting the two payloads had $|\mathbf{v}_g|$ values too small to explain the observed delays in the large n region assuming a smooth horizontally-stratified medium. Thus waves corresponding to such large-n dispersion solutions would arrive well after the OEDIPUS A ionogram display time limit (by approximately a factor of 10) and would not be detected. When the region of smaller n was investigated, labelled "electromagnetic and quasi-electrostatic domain" in Fig. 1.10, and the payloads were assumed to be within an N_e depletion duct (with cross-**B** dimension $\sim$ 100 m), ducted ray paths could be found that were consistent with the observations. James [36] suggested that such ducting may be common in the auroral ionosphere and that it should be considered when trying to interpret natural Z-mode emissions.

The OEDIPUS-C rocket dual-payload was launched from the Poker Flat rocket range in Alaska on November 7, 1995. Again, the sounder-transmitter was on one payload and the sounder-receiver was on the other, and the separation direction between the payloads, now separated by more than a 1 km, differed from the **B** direction by only a few degrees. In this case, James [37] investigated the slow Z-mode propagation corresponding to $f_{pe} < f_{ce} < f < f_{uh}$, i.e., to the CMA-region 3 of Fig. 1.2b. He found, using hot-plasma dispersion theory, that the calculated propagation times for rays directly connecting the observed payloads were typically more than a factor of three greater than the observed time delays between signal transmission and reception.

Thus waves corresponding to such solutions would arrive well beyond the observing time base and would not be detected. In all other cases, there were no solutions corresponding to the desired direction. The received signals could be explained, however, in terms of incoherent Cherenkov and cyclotron radiation from sounder-accelerated electrons (SAE). Particle detectors on both payloads detected SAE following sounder transmissions from the transmitting payload. James [37] could reproduce the observed signal delay times and could predict (within an order of magnitude) the observed signal intensities.

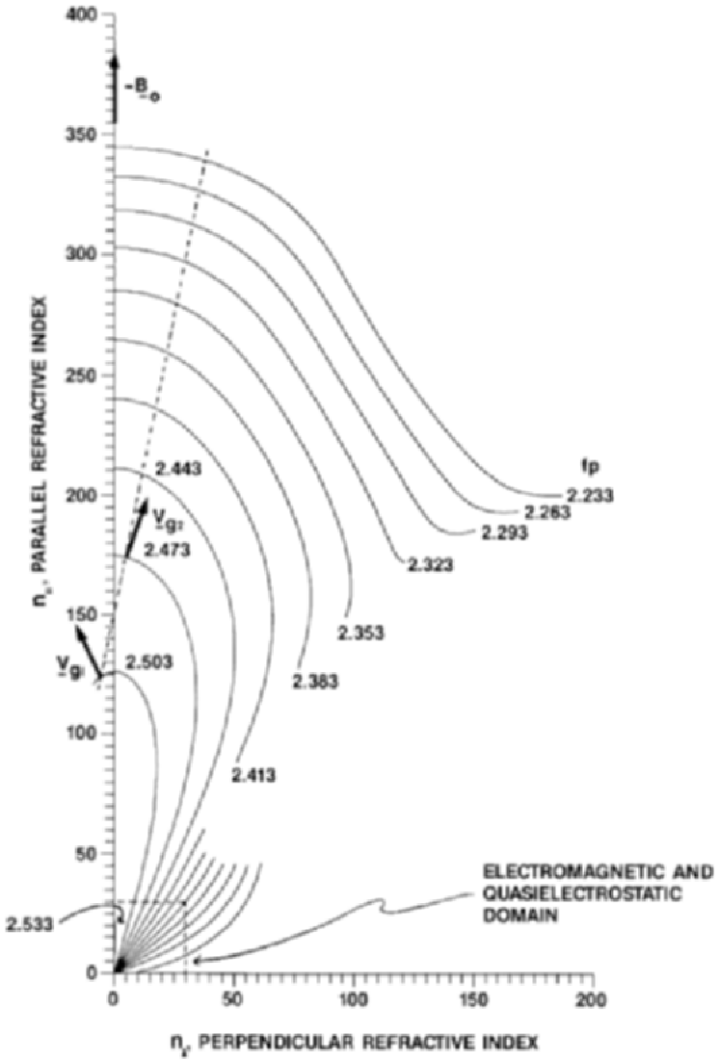

Fig. 1.10. Hot-plasma Z-mode refractive-index surfaces for $f = 2.534\,\mathrm{MHz}$, $f_{ce} = 1.2\,\mathrm{Hz}$, $T_e = 2000\,\mathrm{K}$ and f_{pe}, labelled f_p in the figure, in the range $2.233 = f_{pe} = 2.533\,\mathrm{MHz}$ [James, 36] (Reprinted with permission of the American Geophysical Union)

1.3.5 Dual Payloads: Fast Z

Horita and James [29, 30] investigated fast Z-mode propagation using OEDIPUS-C data corresponding to frequencies below f_{pe} and above the greater of f_Z or f_{ce}, i.e., to CMA-region 4 in Fig. 1.2a where there are no competing cold-plasma wave modes to complicate the interpretation. The Z

mode was found to be stronger than almost all the other cold-plasma modes and to be strongest at frequencies just below f_{pe} for f_{pe}/f_{ce} near and greater than 1 but strongest just above f_Z for higher f_{pe}/f_{ce} values (between 2 and 3). Using cold-plasma dispersion theory, the Balmain [2] antenna-impedance theory and the Kuehl [40] dipole radiation theory they found that the observed and calculated signal intensities were generally in good agreement. They attribute the strength of the Z-mode signals, relative to the other free-space modes, to antenna-impedance values that permit efficient coupling between the antenna and the transmitter and receiver.

1.3.6 Possible Role of Z-Mode Waves in Sounder/Plasma Interactions

Among the plasma instability and nonlinear phenomena stimulated by ionospheric topside sounders investigated by Benson [8] was a diffuse feature observed in the frequency range above the greater of f_{ce} and f_{pe} and below f_{uh}, i.e., in the CMA 3 slow Z-mode regions of Fig. 1.2. It was designated as the DNT resonance because of its generally diffuse appearance on topside ionograms and its location between f_N and f_T (ionospheric notation for f_{pe} and f_{uh}). A weak short-duration (< 1 ms) example of this resonance is shown in Fig. 1.6a. It is often observed for up to about 5 ms. It is not observed over the entire listening range, however, and thus is distinguished from the noise band in this frequency range. This noise band, attributed to wave scattering (see Sect. 1.3.3), is evident in Fig. 1.6a and, more prominently, in Fig. 1.9.

No theoretical interpretation has been offered that explains the frequency and time-duration characteristics of this resonance. It has been attributed by Pulinets [55], Pulinets et al. [56] to the scattering of sounder-generated Z-mode waves and used as a diagnostic tool for the investigation of the distribution of small-scale FAI in the topside ionosphere. James [38] attempted to explain the DNT resonance as observed by the ISIS-II sounder in terms of radiation from SAE in analogy with the successful explanation of Z-mode signals observed by the OEDIPUS-C sounder receiver as described in Sect. 1.3.4. While this explanation was not found to explain the ISIS-II observations, he concluded that SAE may still play a role because SAE pulses that persisted for milliseconds were observed when the OEDIPUS-C sounder transmitter was tuned to the DNT frequencies.

Features have been observed on topside ionograms that imply that ion motions must be considered for a proper interpretation. They appear either as prominent protrusions (called spurs) on the electron resonances (most often from the low-frequency side) or as narrow (in time delay, i.e., apparent range) emissions between the resonances. In either case, they appear with delay times that correspond to multiples of the proton gyroperiod $1/f_{cp}$. One of these phenomena, the proton spurs on the nf_{ce} resonances, appears to be strongly influenced by Z-mode transmissions [Benson, 6]. The spurs are

greatly enhanced when f_Z, from (1.5), is near, but slightly less than, nf_{ce} for $n = 2, 3, 4, \ldots$ and the largest spurs are observed for large n.

Figure 1.6 illustrates the spurs observed on the $3f_{ce}$ resonance when $f_Z \approx 3f_{ce}$. It was suggested that the Z mode may be more efficient at coupling energy into the plasma under these conditions. Note that this frequency region just above f_Z corresponds to the fast Z region where Horita and James [29, 30] found the strongest Z-mode signals which they attributed to optimum antenna-impedance values (see Sect. 1.3.5). Their larger f_{pe}/f_{ce} values, which produce the strongest signals just above f_Z, would correspond to larger f_Z values which, in turn, would correspond to higher nf_{ce} resonances satisfying the condition $f_Z \approx nf_{ce}$; the largest proton spurs were observed under just such conditions [Benson, 6].

Unique Z-mode topside-ionogram signatures have been observed in low latitudes that suggest topside sounders are capable of stimulating, or enhancing, FAI when they encounter the plasma conditions $f_{pe}/f_{ce} \approx n$ where n is an integer larger than 3 [Benson, 10]. An illustration for the case of $n \approx 5$ is presented in Fig. 1.11. Note that well-defined Z, O and X traces are clearly seen for the cases $f_{pe}/f_{ce} < 5$ (top panel) and $f_{pe}/f_{ce} > 5$ (bottom panel) but that the Z trace is masked by a long-duration diffuse signal that extends from f_Z to part way to f_{pe}. It was argued that the frequent occurrence of such signatures made it unlikely that the spacecraft was just encountering FAI when the ambient conditions $f_{pe}/f_{ce} \approx n$ were satisfied. Thus the sounder-generated Z-mode waves were considered to be ducted in FAI stimulated, or enhanced, by the sounder on a short time scale ($\ll 1$ s).

The possibility that this sensitive diagnostic role of the Z-mode waves could be due to efficient scattering when $f_{pe}/f_{ce} \approx n$ was investigated by Zabotin et al. [69]. They did not find any sensitivity in the scattering of Z-mode waves by FAI near the magnetic equator to the conditions $f_{pe}/f_{ce} \approx n$ and concluded that the above examples were either due to sounder stimulation, or enhancement, as proposed or to ducting conditions sensitive to these conditions. No study of the sensitivity of Z-mode ducting by FAI to the conditions $f_{pe}/f_{ce} \approx n$ has been made. As pointed out in Sect. 1.3.2, however, Calvert [17] found that under high N_e conditions (as indicated in Fig. 1.11) Z-mode ducting in the frequency range between f_Z and midway to f_{pe} should be stronger than O- or X-mode ducting, a prediction consistent with the observations in the middle panel of Fig. 1.11. Thus the sensitivity to the $f_{pe}/f_{ce} \approx n$ condition is likely in the generation, or enhancement of existing, FAI by the sounder. Benson [10] gave other examples of sounder-stimulated plasma phenomena when $f_{pe}/f_{ce} \approx n$ and suggested that more energy is deposited into the plasma under these conditions and, particularly, when $f_{pe}/f_{ce} \geq 4$.

Osherovich et al. [52] investigated large-amplitude cylindrical electron oscillations appropriate to FAI, with initial conditions chosen so as to favor Z-mode stimulation, and found that the resulting frequency spectrum was very sensitive to the f_{pe}/f_{ce} value, with larger amplitudes, and more nonlinear frequency components, observed when $f_{pe}/f_{ce} \approx n$, and that the effect

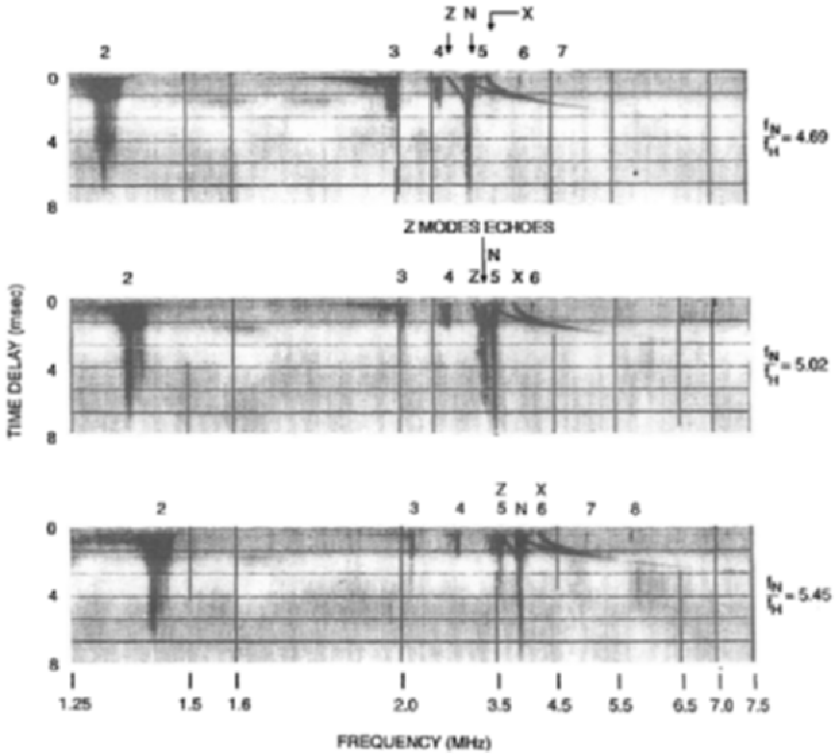

Fig. 1.11. Consecutive Alouette-2 low-latitude ionograms revealing long-duration Z-mode echoes only when $f_{pe}/f_{ce} \approx 5$ at 05:15 UT on 17 June 1969 [Benson, 10]. The label notation is the same as in Fig. 1.7 (Reprinted with permission from Elsevier)

was observed to increase with increasing n. Kuo et al. [41] investigated the creation of FAI by a Z-mode pump wave under the above resonant conditions. They added the constraint that the Z-mode pump wave frequency $f_o \approx f_{pe}$ at a short distance from the satellite where a four-wave coupling process takes place. One of the products in this coupling process corresponds to short-scale (meter size) FAI. They propose that the observed Z-mode diffuse signals, like those in the middle panel of Fig. 1.11, are caused by scattering from these FAI but stress the need for additional research to identify mechanisms that could generate (or enhance) large-scale FAI (>100 m) capable of supporting wave ducting.

1.4 Sounder-Stimulated Z-Mode Waves in the Magnetosphere

1.4.1 Remote O-Z-O-Mode Coupling

Radio sounding in the magnetosphere is challenging because the distances are so large and N_e is so low. These constraints motivated the RPI design for the IMAGE mission. As a result, the IMAGE satellite contains the largest structures ever placed on a spinning satellite, namely, the RPI spin-plane crossed dipole antennas (originally 500 m tip-to-tip length for each). Soon after the IMAGE launch on 25 March 2000 into an elliptical polar orbit, with an apogee of 8 Earth radii (R_E) geocentric distance and a perigee altitude of about 1000 km, the RPI detected discrete long-range echoes outside the plasmasphere in the north polar region. Reinisch et al. [60] and Carpenter et al. [19] attributed them to signals propagating in the X mode in FAI to the polar ionosphere where they were reflected; they were clearly distinguished from the diffuse shorter-range echoes from the nearby highly-irregular plasmapause boundary. Later, echo signatures indicating inter-hemisphere propagation, similar to the ionospheric example shown in Fig. 1.7, were identified by Fung et al. [26]; an example where the Z mode played a prominent role in the interpretation is shown in Fig. 1.12 from Reinisch et al. [61]. This record is called a plasmagram and is the magnetospheric analog of the ionospheric topside-sounder ionogram examples shown in Figs. 1.5–1.9 and 1.11.

The virtual range vs. frequency curves through the data points corresponding to X-mode reflections from the local and conjugate hemispheres (labelled SX and NX, respectively) were used to derive the hemisphere-to-hemisphere N_e distribution along the magnetic field line through the satellite [31]. This field-aligned N_e distribution was then used to calculate the reflections expected for transmitted O-mode signals that coupled to Z-mode signals, which reflected at the distances where the transmitted frequencies were equal to the f_Z cutoff frequencies given by (1.5), and then coupled back to the O-mode signals that were received at the satellite. These O-Z-O traces are labelled NZ and SZ for the echoes of this type from the northern and southern hemispheres, respectively, in Fig. 1.12. This mode-coupling interpretation of Reinisch et al. [61], involving the Z-mode to explain the weaker companion echoes to the inter-hemisphere magnetospheric RPI X-mode echoes, differs from the interpretation of Muldrew [48] of inter-hemisphere ionospheric echoes observed by Alouette 1 in that Muldrew [48] did not invoke O-Z-O mode coupling.

1.4.2 Local Z-Mode Echoes

Echoes of Z-mode signals are often directly observed by RPI in the magnetosphere. Figure 1.13 shows an example when IMAGE was near the plasmapause and a strong N_e gradient could be determined from multiple plasma

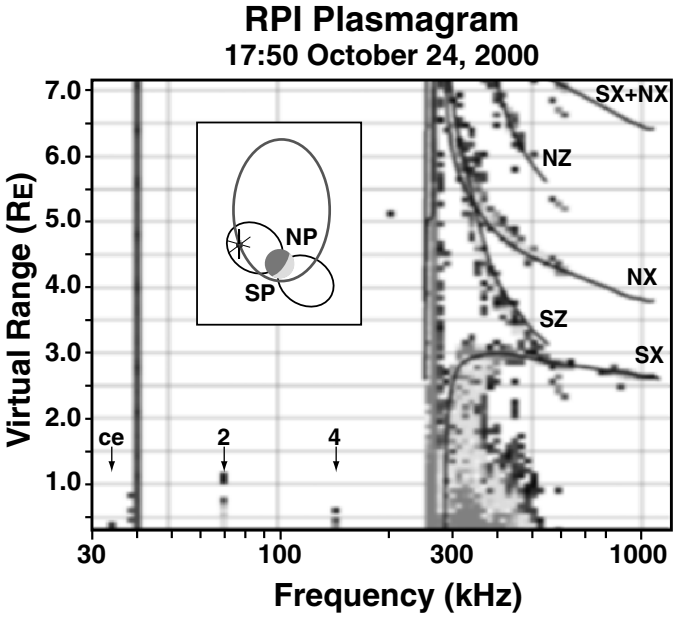

Fig. 1.12. An RPI plasmagram showing echoes from both hemispheres in the frequency region above about 300 kHz, with interpretive traces through the data points, and short-duration plasma resonances at f_{ce}, $2f_{ce}$ and $4f_{ce}$ (lower left). The labels S, N, X, and Z denote southern and northern hemispheres and X and O-Z-O traces respectively. The NX trace has been extrapolated to higher frequencies. The insert shows the orbit, location of IMAGE (x) and the $L = 4$ dipole field lines; NP and SP indicate the magnetic poles [adapted from Reinisch et al., 61] (Reprinted with permission of the American Geophysical Union)

resonances and wave cutoffs. The frequency range of this high-resolution plasmagram fortuitously included the Z- and X-mode cutoffs (f_Z and f_X, respectively) and several plasma resonances. (The linear frequency step size between transmissions of single 3.2 ms pulses was equal to the RPI bandwidth of 300 Hz.) The plasma conditions corresponded to Fig. 1.2a; the Z mode from f_Z to f_{pe} is in CMA region 4 and is the only cold-plasma wave mode. The diffuse nature is attributed to scatter returns from FAI. These scatter returns become more prominent in the CMA region 3 between f_{pe} and f_{uh} (see Fig. 1.2a). This enhanced scatter forms a noise band analogous to the noise band in the ionospheric example of Fig. 1.9 (which, however, corresponds to the CMA 3 region of Fig. 1.2b). Using the values scaled from Fig. 1.13 in (1.3)–(1.5) reveals that consistent solutions cannot be obtained for these equations with constant f_{ce} and f_{pe} values over the 41-s time interval required to record this plasmagram. Three independent f_{pe} determinations can be made, however, if the Tsy 96–1 model magnetic-field values [Tsyganenko, 65, 66, 67],

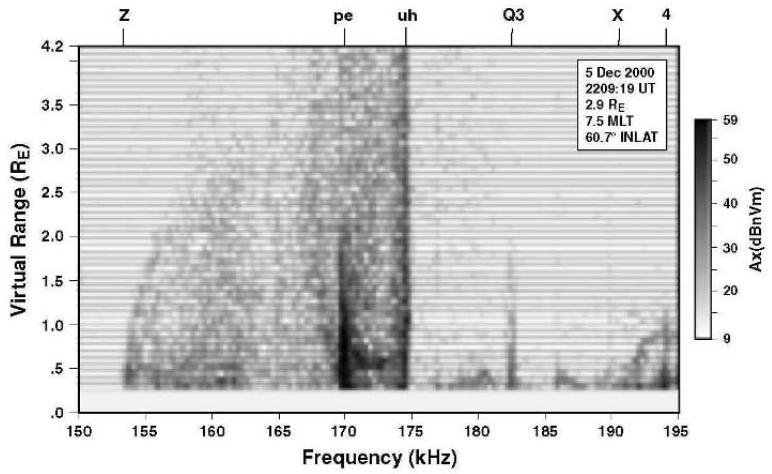

Fig. 1.13. An RPI plasmagram recorded during an outbound plasmapause crossing revealing Z- and X-mode cutoffs and plasma resonances at f_{pe}, f_{uh}, and $4f_{ce}$ labelled at the top by z, x, *pe*, *uh*, and 4, respectively. Also labelled, as $Q3$, at the top is one of the resonances associated with the Bernstein modes discussed in Sect. 1.2 in connection with Fig. 1.4 [adapted from Benson et al. 11] (Reprinted with permission of the American Geophysical Union)

with a percentage offset correction based on the observed $4f_{ce}$ plasma resonance in Fig. 1.13, are used corresponding to the spacecraft locations at the times of the recording of f_Z, f_{uh}, and f_X. The plasma resonance observed at f_{pe} in Fig. 1.13 provides a fourth measurement of f_{pe} and it is independent of the f_{ce} value. While the deduced N_e gradient is large (an order-of-magnitude decrease in a change in L value of approximately 1) [Benson et al., 11], it is only about 1/10 the gradient of a well-developed plasmapause [Carpenter and Anderson, 18].

1.4.3 Z-Mode Refractive-Index Cavities

Among the most spectacular echo signatures observed on RPI plasmagrams are those corresponding to the direct transmission and reception of Z-mode waves that are ducted along FAI within refractive-index cavities [Carpenter et al., 20]. Examples are shown in Fig. 1.14. They were obtained when RPI was operating with a linear frequency step size of 900 Hz. From the observed f_Z values in Fig. 1.14 (corresponding to the onset of the Z-mode traces), and the model values for f_{ce} (off scale to the right in both plasmagrams), it is deduced from (1.5) that f_{pe} is also off scale to the right in both plasmagrams. In both cases, $f_{pe} < f_{ce}$, i.e., propagation corresponding to CMA region 7 in Fig. 1.2b is involved.

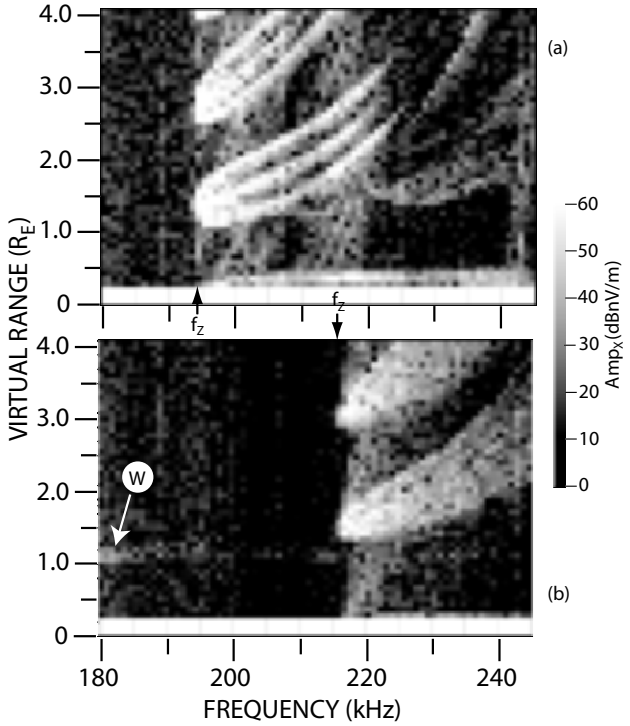

Fig. 1.14. RPI plasmagrams showing multicomponent Z-mode echoes recorded near perigee in the region of N_e gradients between the southern aurora zone and the plasmasphere. (**a**) $L \approx 3.2$, altitude ∼3800 km, $f_Z = 194$ kHz, f_{ce}(model) = 382 kHz implies $f_{pe} \approx 334$ kHz or $f_{pe}/f_{ce} \approx 0.9$; 0824 UT on 26 July 2001. (**b**) $L \approx 2.9$, altitude ∼ 2700 km, $f_Z = 216$ kHz, f_{ce}(model) = 469 kHz implies $f_{pe} \approx 384$ kHz or $f_{pe}/f_{ce} \approx 0.8$; 0245 UT on 12 July 2001 (whistler-mode echoes, due to reflections from the bottom side of the ionosphere [62], are marked "W") [adapted from Carpenter et al. 20] (Reprinted with permission of the American Geophysical Union)

The virtual ranges of the observed echoes starting near 1.5 R_E, which appear as upward slanting epsilons in Figs. 1.14a and 1.14b, are too short to be explained in the same manner as used for the echoes shown in Fig. 1.12, i.e., they are too short to be attributed to echoes from the conjugate hemisphere. They can be explained, however, in terms of ducted echoes returned from within a refractive-index cavity in the hemisphere containing the IMAGE satellite. The interpretation presented by Carpenter et al. [20] is illustrated in Fig. 1.15 for the case when the IMAGE satellite is assumed to be located below a relative minimum in the profile of f_Z along **B**, as deduced from (1.5) with f_{ce} and f_{pe} values based on models and RPI observations.

The most prominent features in Fig. 1.14a are reproduced in Fig. 1.15a with labels corresponding to the ray paths defined in Fig. 1.15b which displays

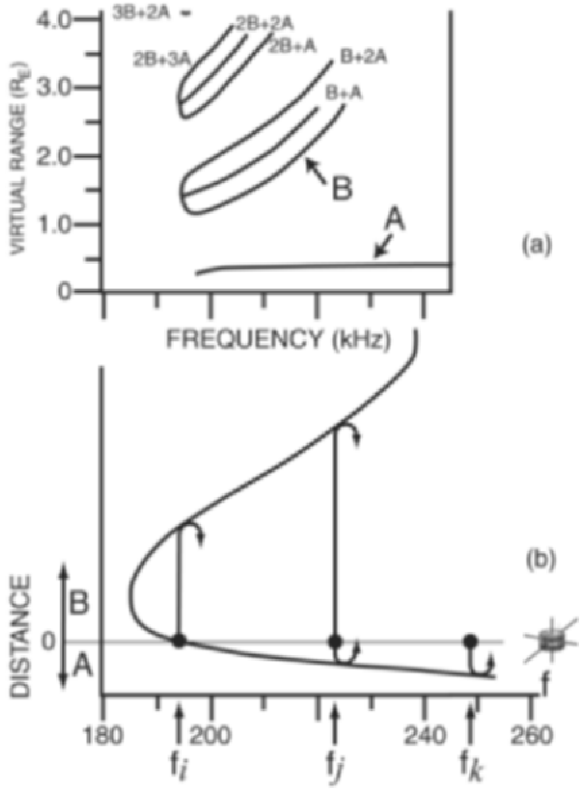

Fig. 1.15. (**a**) Reproduction of the most prominent echoes in Fig. 1.14a. (**b**) Schematic f_Z profile limiting ray paths A and B for representative frequencies f_i, f_j, and f_k, relative to the location of the IMAGE satellite. These ray paths correspond to the labels used for the echo traces in (a) [Carpenter et al., 20] (Reprinted with permission of American Geophysical Union)

an idealized f_Z profile along **B**. When the sounder frequency reaches the frequency f_i, corresponding to the condition $f_i = f_Z$ at the satellite level as illustrated in Fig. 1.15b, a wave can propagate upward along path B into the region where $f_i > f_Z$ and be reflected at a higher altitude where the condition $f_i = f_Z$ is again satisfied. This returning wave is responsible for the echo with a virtual range of $\approx 1.5\,\mathrm{R}_E$, i.e., the nose of the first upward slanting epsilon signature in Fig. 1.15a. This wave is reflected again at the $f_i = f_Z$ condition at the satellite and the process is repeated. Two such repetitions are evident in the data of Fig. 1.14a and the reproduction in Fig. 1.15a. Higher sounder frequencies, such as f_j in Fig. 1.15b, correspond to the condition $f_j > f_Z$ at the satellite level, and waves can now propagate both upward along path B and downward along path A, within the region where $f_j > f_Z$, and be reflected at both higher and lower altitudes where the condition $f_j = f_Z$

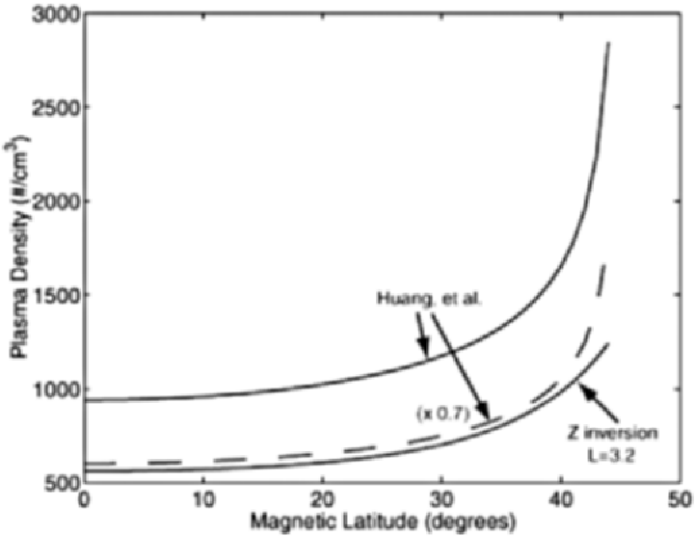

Fig. 1.16. N_e along the $L = 3.2$ magnetic-field line above the IMAGE satellite derived from inverting the "B" Z trace of Fig. 1.15a compared with an RPI-derived empirical model of Huang et al. [31] for a different day (8 June 2001) and a scaling of that model by a factor of 0.7. The portion of the lowest curve corresponding to magnetic latitude values less than 13° is an extrapolation [Carpenter et al. 20] (Reprinted with permission of the American Geophysical Union)

is satisfied. Multiple combinations of these echoes produced the elements of the epsilon signatures seen in Figs. 1.14a and 1.15a. Carpenter et al. [20] also presented examples of a special form of echo signature on RPI plasmagrams that corresponds to ducted Z-mode propagation along FAI within Z-mode refractive-index cavities when IMAGE is assumed to be located above the relative minimum in the profile of f_Z along $\mathbf{B}$.

Carpenter et al. [20] introduced an inversion method to determine the N_e distribution along $\mathbf{B}$ from the upward propagating signals within Z-mode refractive-index cavities of the type discussed above. The results of applying this method to the trace corresponding to B in Fig. 1.15a are presented in Fig. 1.16. Also presented in Fig. 1.16 are predicted values from an empirical N_e model based on the inversion of RPI X-mode echoes from signals that propagated on multiple field-aligned paths on a different day, namely, 8 June 2001 [Huang et al., 31]. The lower N_e values derived from the Z-mode data were attributed to the movement of IMAGE through a region of plasmapause N_e gradients at the time of the measurements. Since these Z-mode echoes from waves trapped in Z-mode refractive-index cavities are often the only prominent echoes observed on a single plasmagram, this inversion method provides a valuable diagnostic tool for determining the N_e distribution along $\mathbf{B}$.

1.4.4 Whistler- and Z-Mode Echoes

In an investigation of IMAGE/RPI data in the inner plasmasphere and at moderate to low altitudes over the polar regions, Sonwalkar et al. [62] found diffuse Z-mode echoes often accompanied whistler (W)-mode echoes. An example from their study is shown in Fig. 1.17. The W-mode echo in this figure, with narrowly defined time delay as a function of frequency, is an example of a discrete echo. The Z-mode echo, with a time-delay spread that increases with frequency, is an example of a diffuse echo. As discussed by Carpenter et al. [20], this Z-mode pattern is characteristic of the low altitude polar region and the plasma condition $f_{pe}/f_{ce} < 1$. The abrupt high-frequency cutoff of this Z-mode echo, and the long-duration sounder-stimulated plasma resonance at ∼787 kHz in Fig. 1.17, provides a measure of f_{uh} [Benson et al., 14]; the gap, or decrease in echo spreading at ∼685 kHz, provides a measure of f_{ce} [Carpenter et al., 20]. From these values f_{pe} is calculated to be ∼387 kHz from (1.3).

Whistler-mode echoes with a much broader range of time delays with frequency than those shown in Fig. 1.17 are also observed on IMAGE. They are called diffuse W-mode echoes [Sonwalkar et al., 62]. In regions poleward of the plasmasphere, diffuse Z-mode echoes of the kind illustrated in Fig. 1.17 were found to accompany both discrete and diffuse W-mode echoes 90% of the time, and were also present during 90% of the soundings when no W-mode echoes were detected.

Based on comparisons of ray tracing simulations with the observed dispersion of W- and Z-mode echoes, Sonwalkar et al. [62] proposed that: (1) the observed discrete W-mode echoes are due to RPI signal reflections from the

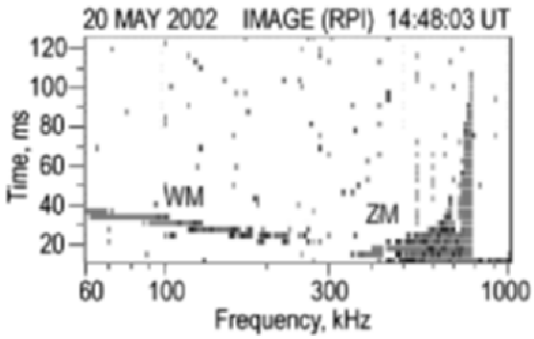

Fig. 1.17. RPI plasmagram displaying both W-mode echoes (frequencies below ∼300 kHz) and diffuse Z-mode echoes (frequencies above ∼300 kHz) labelled WM and ZM, respectively. The minimum observable time delay is 13 ms due to the 3.2-ms minimum transmitted pulse length and additional time needed for the receiver to recover from the high voltage generated during the transmitter pulses. The amplitude scale is coded from 10 to 50 dB nV/m [adapted from Sonwalkar et al., 62] (Reprinted with permission of the American Geophysical Union)

lower boundary of the ionosphere, (2) the diffuse W-mode echoes are due to scattering of RPI signals by FAI located within 2000 km earthward of IMAGE and in directions close to that of the field line passing through IMAGE, and (3) the diffuse Z-mode echoes are due to scattering of RPI signals from FAI within 3000 km of IMAGE, particularly to signals propagating in the generally cross-**B** direction.

This interpretation suggests that Z-mode echoes occur most frequently ($\sim 90\%$), both in the presence and absence of whistler-mode echoes, because the Z-mode waves capable of returning to the sounder can propagate long distances in all directions, i.e., not only close to the field lines as in the case of the whistler mode waves that are capable of returning to the sounder. Thus there is a much larger probability of encountering plasma irregularities which may lead to Z-mode echoes. These RPI results are consistent with previous investigations in that they indicate that the high-latitude magnetosphere is highly structured with FAI that exist over cross-**B** scales ranging from 10 m to 100 km and that these FAI profoundly effect W- and Z-mode propagation.

1.5 Active/Passive Investigation of Z-Mode Waves of Magnetospheric Origin

The first observation of enhanced Z-mode radio emissions of natural origin, corresponding to CMA-region 3 in Fig. 1.2, were made during the radio-astronomy rocket experiment of Walsh et al. [68]. They ruled out a thermal source due to the large signal intensities and suggested Cherenkov radiation as a likely source mechanism because of the large refractive index (and hence low wave phase velocities) in this frequency domain. Bauer and Stone [3], using satellite observations, were the first to show that the observed frequency limits of this CMA region 3 Z-mode radiation could be used to determine the magnetospheric N_e. Several later experiments have investigated these emissions attributed to CMA region 3 Z-mode radiation by comparing the observed frequencies with f_{pe} values determined by active techniques. Beghin et al. [4] used the AUREOL/ARCADE-3 mutual impedance probe in the 400–2000 km altitude region, Kurth et al. [42] used a sounder during a brief (5 min) period of the single pass through the terrestrial magnetosphere by Cassini, and Benson et al. [12] used active soundings by the RPI on four passes of IMAGE in the vicinity of the plasmapause region.

In each of these investigations, it was concluded that the upper and lower frequency boundaries of an observed intense upper-hybrid band corresponded to f_{uh} and f_{pe}, respectively, in the region where $f_{pe} > f_{ce}$. In the study by Benson et al. [12] these frequency identifications were found to hold to an accuracy of a few per cent in f_{pe} by interpolating between active soundings to the intervening passive dynamic spectra. Figure 1.18 shows the results of superimposing the plasmagram-determined f_{ce}, f_{pe} and f_{uh} values from active

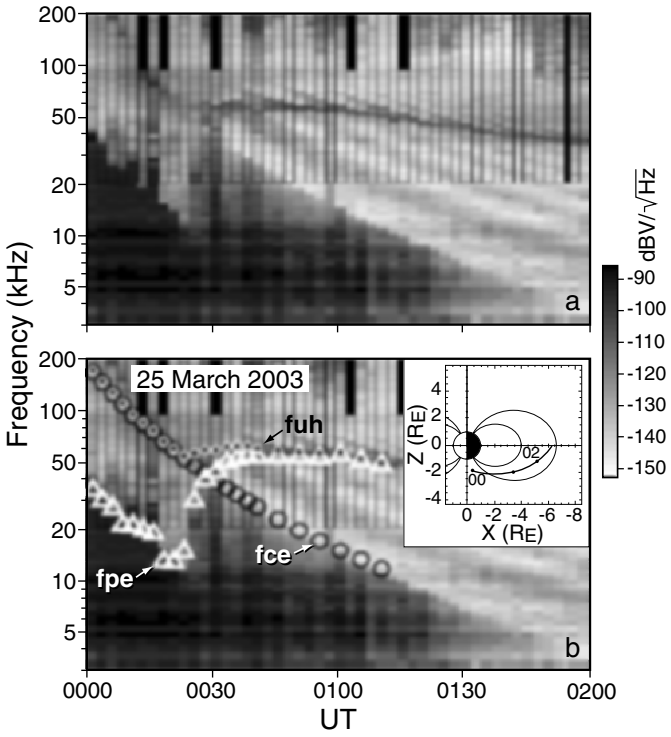

Fig. 1.18. (**a**) Passive RPI dynamic spectrum. (**b**) Same as (a) except with superimposed f_{ce}, f_{pe} and f_{uh} values determined from active RPI plasmagrams [adapted from Benson et al., 12] (Reprinted with permission of the American Geophysical Union)

sounding on the passive RPI dynamic spectrum corresponding to the same time interval.

Comparing Figs. 1.18a and 1.18b illustrates the benefit of having active soundings to confidently determine f_{pe}, particularly when $f_{pe} < f_{ce}$. The sounder-derived f_{pe} values (white triangles) follow the upper edge of an intense, presumably whistler mode, emission. They deviate from this upper edge, however, at a location that would be difficult to determine without the active soundings. Also, in this $f_{pe} < f_{ce}$ frequency domain, the upper-hybrid band enhancement, in this case between f_{ce} and f_{uh}, is often not very well defined as f_{uh} approaches f_{ce}. Beghin et al. [4] never observed an enhancement when $f_{pe} < f_{ce}$; they attribute this finding to a lack of instability growth of Z-mode waves in the upper-hybrid band under these conditions. The upper-hybrid band is relatively broad (extending from ∼50 to 60 kHz) near 00:30 UT where $f_{pe} \sim f_{ce}$, and it narrows in bandwidth as time progresses. The scaled f_{pe} and f_{uh} frequencies in the region beyond about 00:30 UT, i.e., in the region

where $f_{pe} > f_{ce}$, allow the boundaries of the upper-hybrid band to be identified and distinguished from the slanting finger-like higher-frequency emissions which are attributed to Bernstein-mode emissions discussed in connection with Fig. 1.4.

Figure 1.18 suggests that there are two different sources of the observed W-mode emissions, one more intense than the other. The most intense one extends out to slightly beyond 01:00 UT and is limited by the minimum in f_{pe} near 10 kHz as determined from the active sounding. The weaker one extends out to about 01:45 UT and is limited by f_{ce} from this point backward in time to 00:30 where it is limited by f_{pe}. At earlier times, the weak emissions in the frequency domain from f_{pe} to f_{uh} could be either L-O or CMA region 6 a Z-mode emissions (see Fig. 1.2b).

Confirming identifications of passive dynamic-spectral features by nearly-simultaneous active determinations of f_{pe}, such as illustrated in Fig. 1.18, provides confidence in the interpretation of the passive dynamic spectra when supporting active measurements are not available. It also provides confidence in the use of the passive dynamic spectra to help interpret plasmagrams when the spectrum of sounder-stimulated resonances is complex [Benson et al., 11].

1.6 Summary

Even though the Z mode is an internal, or trapped, mode of the plasma it has valuable diagnostic applications in space plasmas in both active and passive wave experiments. In active experiments discrete Z-mode echo traces can be inverted to provide N_e profiles, diffuse traces provide information about FAI, and two-point propagation studies provide information concerning wave propagation, wave ducting and wave/particle interactions. In passive experiments, intense Z-mode signals of magnetospheric origin provide valuable ambient N_e information.

Acknowledgements

We are grateful to the reviewer for many helpful comments on the manuscript. The work at the University of Alaska Fairbanks was supported by NASA under contract NNG04GI67G. Support for B. W. R. was provided by NASA under subcontract 83822 from SwRI.

References

[1] Allis, W.P., S.J. Buchsbaum, and A. Bers: Waves in anisotropic plasmas, MIT Press, Cambridge, 1963.

[2] Balmain, K.G.: Dipole admittance for magnetoplasma diagnostics, IEEE Trans. Antennas Propag. 17, 389–392, 1969.
[3] Bauer, S.J. and R.G. Stone: Satellite observations of radio noise in the magnetosphere, Nature 218, 1145–1147, 1968.
[4] Beghin, C., J.L. Rauch, and J.M. Bosqued: Electrostatic plasma waves and HF auroral hiss generated at low altitude, J. Geophys. Res., 94, 1359–1379, 1989.
[5] Beghin, C., J.L. Rauch, and J.M. Bosqued: Electrostatic plasma waves and HF auroral hiss generated at low altitude, J. Geophys. Res. 94, 1359–1379, 1989.
[6] Benson, R.F.: Ion effects on ionospheric electron resonance phenomena, Radio Sci. 10, 173–185, 1975.
[7] Benson, R.F.: Stimulated plasma waves in the ionosphere, Radio Sci. 12, 861–878, 1977.
[8] Benson, R.F.: Stimulated plasma instability and nonlinear phenomena in the ionosphere, Radio Sci. 17, 1637–1659, 1982.
[9] Benson, R.F.: Field-aligned electron density irregularities near 500 km – Equator to polar cap topside sounder Z mode observations, Radio Sci. 20, 477–485, 1985.
[10] Benson, R.F.: Evidence for the stimulation of field-aligned electron density irregularities on a short time scale by ionospheric topside sounders, J. Atm. and Solar-Terr. Phys. 59, 2281–2293, 1997.
[11] Benson, R.F., V.A. Osherovich, J. Fainberg, and B.W. Reinisch: Classification of IMAGE/RPI-stimulated plasma resonances for the accurate determination of magnetospheric electron-density and magnetic field values, J. Geophys. Res. 108, 1207, doi:10.1029/2002JA009589, 2003.
[12] Benson, R.F., P.A. Webb, J.L. Green, L. Garcia, and B.W. Reinisch: Magnetospheric electron densities inferred from upper-hybrid band emissions, Geophys. Res. Lett. 31, L20803,doi:1029/2004GL020847, 2004.
[13] Bernstein, I.B.: Waves in a plasma in a magnetic field, Phys. Rev. 109, 10–21, 1958.
[14] Budden, K.G.: The propagation of radio waves, the theory of radio waves of low power in the ionosphere and magnetosphere, 669 pp., Cambridge University Press, New York, 1985.
[15] Burch, J.L.: The first two years of IMAGE, Space Sci. Rev. 109, 1–24, 2003.
[16] Calvert, W., Oblique z-mode echoes in the topside ionosphere, J. Geophys. Res. 71, 5579–5583, 1966.
[17] Calvert, W.: Wave ducting in different wave modes, J. Geophys. Res., 100 (A9), 17,491–17,497, 1995.
[18] Carpenter, D.L. and R.R. Anderson: An ISEE/whistler model of equatorial electron density in the magnetosphere, J. Geophys. Res. 97, 1097–1108, 1992.
[19] Carpenter, D.L., M.A. Spasojevic, T.F. Bell, U.S. Inan, B.W. Reinisch, I.A. Galkin, R.F. Benson, J.L. Green, S.F. Fung, and S.A. Boardsen: Small-scale field-aligned plasmaspheric density structures inferred from RPI on IMAGE, J. Geophys. Res., 107(A9), 1258, doi:10.1029/2001JA009199, 2002.
[20] Carpenter, D.L., T.F. Bell, U.S. Inan, R.F. Benson, V.S. Sonwalkar, B.W. Reinisch, and D.L. Gallagher: Z-mode sounding within propagation "cavities" and other inner magnetospheric regions by the RPI instrument on the IMAGE satellite, J. Geophys. Res. 108, 1421, doi:10.1029/2003JA010025, 2003.

[21] Denisenko, P.F., N.A. Zabotin, D.S. Bratsun, and S.A. Pulinets: Detection and mapping of small-scale irregularities by topside sounder data, Ann. Geophysicae 11, 595–600, 1993.
[22] Dyson, P.L. and R.F. Benson: Topside sounder observations of equatorial bubbles, Geophys. Res. Lett. 5, 795–798, 1978.
[23] Eckersley, T.L.: Discussion of the ionosphere, Proc. Roy. Soc. A141, 708–715, 1933.
[24] Ellis, G.R.: The Z propagation hole in the ionosphere, J. Atmosph. Terr. Phys. 8, 43–54, 1956.
[25] Franklin, C.A. and M.A. Maclean: The design of swept-frequency topside sounders, Proc. IEEE 57, 897–929, 1969.
[26] Fung, S.F., R.F. Benson, D.L. Carpenter, J.L. Green, V. Jayanti, I.A. Galkan, and B.W. Reinisch: Guided Echoes in the Magnetosphere: Observations by Radio Plasma Imager on IMAGE, Geophys. Res. Lett. 3, 1589, doi:10.1029/2002GL016531, 2003.
[27] Goertz, C.K. and R.J. Strangeway: Plasma waves, in: Introduction to Space Physics, edited by M.G. Kivelson, and C.T. Russell, pp. 356–399, Cambridge University Press, New York, 1995.
[28] Gurnett, D.A., S.D. Shawhan, and R.R. Shaw: Auroral hiss, Z mode radiation, and auroral kilometric radiation in the polar magnetosphere: DE 1 observations, J. Geophys. Res. 88, 329–340, 1983.
[29] Horita, R.E. and H.G. James: Enhanced Z-mode radiation from a dipole, Adv. Space Res. 29, 1375–1378, 2002.
[30] Horita, R.E. and H.G. James: Two-point studies of fast Z-mode waves with dipoles in the ionosphere, Radio Sci., 39, RS4001, doi:10.1029/2003RS002994, 2004.
[31] Huang, X., B.W. Reinisch, P. Song, P. Nsumei, J.L. Green, and D.L. Gallagher: Developing an empirical density model of the plasmasphere using IMAGE/RPI observations, Adv. Space Res. 33, 829–832, 2004.
[32] Jackson, J.E.: The reduction of topside ionograms to electron-density profiles, Proc. IEEE 57, 960–976, 1969.
[33] Jackson, J.E. and E.S. Warren: Objectives, history, and principal achievments of the topside sounder and ISIS programs, Proc. IEEE 57, 861–865, 1969.
[34] James, H.G.: Wave propagation experiments at medium frequencies between two ionospheric satellites, 1, General results, Radio Sci. 13, 531–542, 1978.
[35] James, H.G.: Wave propagation experiments at medium frequencies between two ionospheric satellites 3. Z mode pulses, J. Geophys. Res. 84, 499–506, 1979.
[36] James, H.G.: Guided Z mode propagation observed in the OEDIPUS A tethered rocket experiment, J. Geophys. Res. 96, 17,865–17,878, 1991.
[37] James, H.G.: Slow Z-mode radiation from sounder-accelerated electrons, J. Atmos. Solar-Terr. Phys. 66, 1755–1765, 2004.
[38] James, H.G., Radiation from sounder-accelerated electrons, Adv. Space Res., in press, 2005.
[39] Kelso, J.M.: Radio ray propagation in the ionosphere, 408 pp., McGraw Hill, New York, 1964.
[40] Kuehl, H.H.: Electromagnetic radiation from an electric dipole in a cold anisotropic plasma, Phys. Fluids 5, 1095–1103, 1962.

[41] Kuo, S.P., M.C. Lee, and P. Kossey: Excitation of short-scale field-aligned electron density irregularities by ionospheric topside sounders, J. Geophys. Res. 104, 19,889–19,894, 1999.
[42] Kurth, W.S., G.B. Hospodarsky, D.A. Gurnett, M.L. Kaiser, J.-E. Wahlund, A. Roux, P. Canu, P. Zarka, and Y. Tokarev: An overview of observations by the Cassini radio and plasma wave investigation at Earth, J. Geophys. Res. 106, 30239–30252, 2001.
[43] LaBelle, J. and R.A. Treumann: Auroral radio emissions, 1. hisses, roars, and bursts, Space Sci. Rev. 101, 295–440, 2002.
[44] Lewis, R.M. and J.B. Keller: Conductivity tensor and dispersion equation for a plasma, Phys. Fluids, 5, 1248–1264, 1962.
[45] Lockwood, G.E.K.: A ray-tracing investigation of ionospheric Z-mode propagation, Can. J. Phys. 40, 1840–1843, 1962.
[46] McAfee, J.R.: Ray trajectories in an anisotropic plasma near plasma resonance, J. Geophys. Res. 73, 5577–5583, 1968.
[47] McAfee, J.R.: Topside ray trajectories near the upper hybrid resonance, J. Geophys. Res. 74, 6403–6408, 1969.
[48] Muldrew, D.B.: Radio propagation along magnetic field-aligned sheets of ionization observed by the Alouette topside sounder, J. Geophys. Res. 68, 5355–5370, 1963.
[49] Muldrew, D.B.: Nonvertical propagation and delayed-echo generation observed by the topside sounders, Proc. IEEE 57, 1097–1107, 1969.
[50] Muldrew, D.B.: Electron resonances observed with topside sounders, Radio Sci. 7, 779–789, 1972.
[51] Muldrew, D.B. and M.F. Estabrooks: Computation of dispersion curves for a hot magnetoplasma with application to the upper-hybrid and cyclotron frequencies, Radio Sci. 7, 579–586, 1972.
[52] Osherovich, V.A., J. Fainberg, R.F. Benson, and R.G. Stone: Theoretical analysis of resonance conditions in magnetized plasmas when the plasma/gyro frequency ratio is close to an integer, J. Atm. and Solar-Terr. Phys. 59, 2361–2366, 1997.
[53] Oya, H.: Conversion of electrostatic plasma waves into electromagnetic waves: numerical calculation of the dispersion relation for all wavelengths, Radio Sci. 6, 1131–1141, 1971.
[54] Poeverlein, H.: Strahlwege von Radiowellen in der Ionosphäre, Z. Angew. Phys. 1, 517, 1949.
[55] Pulinets, S.A.: Prospects of topside sounding, in WITS handbook N2, edited by C.H. Liu, pp. 99–127, SCOSTEP Publishing, Urbana, Illinois, 1989.
[56] Pulinets, S.A., P.F. Denisenko, N.A. Zabotin, and T.A. Klimanova: New method for small-scale irregularities diagnostics from topside sounder data, in: SUNDIAL Workshop, McLean, Virginia, 1989.
[57] Ratcliffe, J.A.: The Magneto-Ionic Theory and its Applications to the Ionosphere, 206 pp., Cambridge University Press, New York, 1959.
[58] Reinisch, B.W.: Modern Ionosondes, in: Modern Ionospheric Science, edited by H. Kohl, R. Ruster, and K. Schlegel, pp. 440–458, European Geophysical Society, Katlenburg-Lindau, Germany, 1996.
[59] Reinisch, B.W., D.M. Haines, K. Bibl, G. Cheney, I.A. Gulkin, X. Huang, S.H. Myers, G.S. Sales, R.F. Benson, S.F. Fung, J.L. Green, W.W.L. Taylor, J.-L. Bougeret, R. Manning, N. Meyer-Vernet, M. Moncuquet, D.L. Carpenter, D.L.

Gallagher, and P. Reiff: The radio plasma imager investigation on the IMAGE spacecraft, Space Sci. Rev. 91, 319–359, 2000.

[60] Reinisch, B.W., X. Huang, D.M. Haines, I.A. Galkin, J.L. Green, R.F. Benson, S.F. Fung, W.W.L. Taylor, P.H. Reiff, D.L. Gallagher, J.-L. Bougeret, R. Manning, D.L. Carpenter, and S.A. Boardsen: First results from the radio plasma imager on IMAGE, Geophys. Res. Lett. 28, 1167–1170, 2001a.

[61] Reinisch, B.W., X. Huang, P. Song, G.S. Sales, S.F. Fung, J.L. Green, D.L. Gallagher, and V.M. Vasyliunas: Plasma density distribution along the magnetospheric field: RPI observations from IMAGE, Geophys. Res. Lett. 28, 4521–4524, 2001b.

[62] Sonwalkar, V.S., D.L. Carpenter, T.F. Bell, M.A. Spasojevic, U.S. Inan, J. Li, X. Chen, A. Venkatasubramanian, J. Harikumar, R.F. Benson, W.W.L. Taylor, and B.W. Reinisch: Diagnostics of magnetospheric electron density and irregularities at altitudes <5000 km using whistler and Z mode echoes from radio sounding on the IMAGE satellite, J. Geophys. Res. 109, A11212, doi:10.1029/2004JA010471, 2004.

[63] Stix, T.H.: The Theory of Plasma Waves, 283 pp., McGraw-Hill, New York, 1962.

[64] Thomas, J.O.: The distribution of electrons in the ionosphere, Proc. IRE 47, 162–175, 1959.

[65] Tsyganenko, N.A.: Modeling the Earth's magnetospheric magnetic field confined within a realistic magnetopause, J. Geophys. Res. 100, 5599–5612, 1995.

[66] Tsyganenko, N.A.: Effects of the solar wind conditions on the global magnetospheric configuration as deduced from data-based field models, in 3rd International Conference on Substorms (ICS-3), pp. 181–185, ESA SP-389, Versailles, France, 1996.

[67] Tsyganenko, N.A. and D.P. Stern: Modeling the global magnetic field of the large-scale Birkeland current systems, J. Geophys. Res. 101, 27,187–27,198, 1996.

[68] Walsh, D., F.T. Haddock, and H.F. Schulte: Cosmic radio intensities at 1.225 and 2.0 Mc measured up to an altitude of 1700 km, in: Space Research, edited by P. Muller, pp. 935–959, North Holland Publishing Company, Amsterdam, 1964.

[69] Zabotin, N.A., D.S. Bratsun, S.A. Pulinets, and R.F. Benson: Response of topside radio sounding signals to small-scale field-aligned ionospheric irregularities, J. Atmosph. Solar-Terr. Phys. 59, 2231–2246, 1997.